

# Rocket Plume Scaling for Orion Wind Tunnel Testing

Gregory J. Brauckmann<sup>1</sup>

*NASA Langley Research Center, Hampton, VA 23681*

James S. Greathouse<sup>2</sup> and Molly E. White<sup>3</sup>

*NASA Johnson Space Center, Houston, TX 77058*

**A wind tunnel test program was undertaken to assess the jet interaction effects caused by the various solid rocket motors used on the Orion Launch Abort Vehicle (LAV). These interactions of the external flowfield and the various rocket plumes can cause localized aerodynamic disturbances yielding significant and highly non-linear control amplifications and attenuations. This paper discusses the scaling methodologies used to model the flight plumes in the wind tunnel using cold air as the simulant gas. Comparisons of predicted flight, predicted wind tunnel, and measured wind tunnel forces-and-moments and plume flowfields are made to assess the effectiveness of the selected scaling methodologies.**

## Nomenclature

$A_e$	=	nozzle exit area, ft <sup>2</sup>
$C_{T,v}$	=	thrust coefficient
$M_e$	=	jet exit Mach number
$M_{fe}$	=	fully-expanded Mach number
$M_\infty$	=	freestream Mach number
$P_e$	=	jet exit static pressure, psf
$q_{fe}$	=	fully-expanded dynamic pressure, psf
$q_\infty$	=	freestream dynamic pressure, psf
$R_j$	=	jet gas constant, ft-lbf / lbm-°R
$R_\infty$	=	freestream gas constant, ft-lbf / lbm-°R
$S$	=	vehicle reference area, ft <sup>2</sup>
$T_e$	=	jet exit static temperature, °R
$T_v$	=	nozzle vacuum thrust, lbf
$T_\infty$	=	freestream static temperature, °R
$V_e$	=	jet exit velocity, ft/s
$V_\infty$	=	freestream velocity, ft/s
$\alpha$	=	angle of attack, deg
$\beta_j$	=	jet Mach number function, $\sqrt{M_e^2 - 1}$
$\beta_\infty$	=	freestream Mach number function, $\sqrt{M_\infty^2 - 1}$
$\gamma_j$	=	jet ratio of specific heats
$\gamma_\infty$	=	freestream ratio of specific heats
$\Delta C_m$	=	pitching-moment increment
$\theta_e$	=	nozzle exit half-angle, deg
$\theta_i$	=	thrust direction for individual nozzle, deg
$\theta_r$	=	resultant thrust direction, deg
AMCT	=	abort motor thrust coefficient (defined in paper)
ACMTR	=	attitude control motor thrust ratio (defined in paper)
ACMTB	=	attitude control motor thrust balance (defined in paper)

<sup>1</sup> Aerospace engineer, Aerothermodynamics Branch, MS408A, Associate Fellow AIAA.

<sup>2</sup> Aerospace engineer, Applied Aeroscience and CFD Branch, EG3.

<sup>3</sup> Aerospace engineer, Applied Aeroscience and CFD Branch, EG3, Member AIAA.

## I. Introduction

THE Apollo-derived Orion Crew Exploration Vehicle (CEV) is part of NASA's now-cancelled Constellation Program to return humans to the moon and other destinations in the solar system. Although Constellation is cancelled, work continues on the Orion spacecraft as it may be used in future NASA programs.

To maximize the crew's safety, Orion will include a Launch Abort System (LAS) capable of pulling the spacecraft and its crew to safety in the event of an emergency on the launch pad or at any time during ascent. The LAS mated with the Crew Module (CM) constitutes the Launch Abort Vehicle (LAV) configuration planned for operational use (Fig. 1). The LAS consists of an ogive-conical fairing surrounding the CM, an abort motor (AM) to provide the main propulsive force to accelerate the vehicle, a jettison motor (JM) to separate the LAS from the CM once the vehicle is clear of the launch vehicle, and an attitude control motor (ACM) to provide steering torques for the LAV.

A typical abort event sequence is shown in Fig. 2. Throughout this paper the different phases of flight will be referred to as "boost phase", when the main abort motors are operating along with the ACM steering motors, "coast phase" when only the ACM motors are operating before re-orientation begins and the LAV is at relatively low angles of attack, "re-orientation" begins when the ACM motors steer the LAV to flip from tower-forward to heat-shield-forward flight, and "tower-jettison phase" is when the LAS tower separates from the CM to expose the parachute system, using the jettison motors.

All three motors (AM, ACM, JM) use a solid propellant. The ACM is a set of 8 circumferential nozzles near the nose of the vehicle. The nozzles are fed by a common combustion chamber and the thrust of each nozzle is individually controlled by a set of pintles that move in and out to vary the throat areas. Total available thrust in any specific direction varies, with a maximum of around 7500 pounds. The AM is a reverse-flow design encompassing the lower portion of the LAS tower. The reverse flow design saves weight compared to an Apollo-type system where the exhaust exits from the bottom requiring a tower standoff to move the exhaust plumes away from the CM. As with the ACM the AM nozzles are fed by a common combustion chamber. Thrust is on the order of 400,000 pounds. The AM nozzles are configured with inserted liners that vary the throat diameters in order to create a thrust offset. The thrust offset is used to align the thrust vector with the vehicle center of gravity. The JM is located above the abort motors and exhausts through 4 scarfed nozzles. The JM nozzles are designed with different throat diameters in order to create a thrust offset, necessary to move the LAS away from the launch vehicle flight path when it is jettisoned during a nominal (non-abort) ascent. Thrust from the JM is around 40,000 pounds.

As with all jets, the vehicle flowfield is altered by the presence of the exhaust plumes. It is necessary to assess the effects of these jet-interactions (JI) between the various ACM, AM, and JM exhaust plumes and the external flow

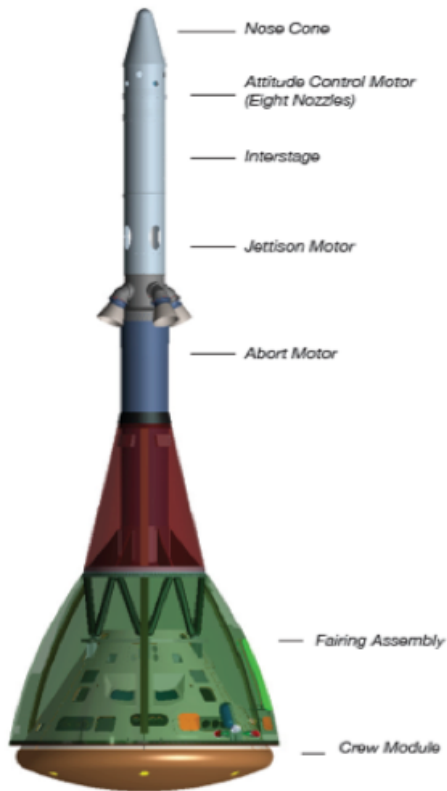


Figure 1. LAS-606-ALAS and Orion crew module

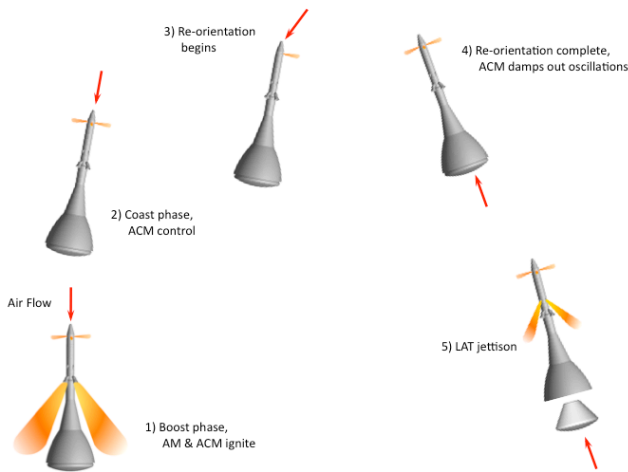


Figure 2. Typical abort sequence

along the outside surfaces of the LAV. The complex JI effects are expected to result in localized aerodynamic disturbances as well as downstream effects that can yield significant and highly non-linear control amplifications and attenuations. These changes in flight control characteristics must be accounted for in developing LAV flight characteristics.

This paper describes the design of nozzles for use in a wind tunnel test program to assess the various plume interaction effects. Wind tunnel tests typically use a simulant gas to model the actual rocket exhaust plumes. The Orion CEV wind tunnel test program used cold high-pressure air due to its immediate availability at the facilities. Proper scaling is necessary to account for the differences between cold air and the actual hot exhaust gases and pure geometric scaling is not appropriate. Many parameters can be used to provide similarity between the wind tunnel nozzle flow and flight, such as momentum flux ratio or exit pressure ratio, and each attempts to capture a different aspect of the plume/flowfield interaction<sup>1-5</sup>. The plume boundary (size and shape of the plume) is primarily a blockage effect and is scaled by the exit pressure ratio. The plume trajectory (distance and location of the plume penetration) is scaled by the momentum flux ratio. Plume entrainment and mixing (mass or energy transfer along the plume edge) is scaled by the velocity or kinetic energy ratio. From Ref. 1, these terms are:

- 1) Plume boundary (exit pressure ratio):  $\frac{\gamma_j M_e^2}{\gamma_\infty M_\infty^2}$  or  $\frac{\gamma_j M_e^2 / \beta_j}{\gamma_\infty M_\infty^2 / \beta_\infty}$
- 2) Plume trajectory (momentum flux ratio):  $\frac{\rho_e A_e V_e^2}{\rho_\infty A_e V_\infty^2}$
- 3) Plume entrainment (kinetic energy or velocity ratio):  $\frac{R_j T_e}{R_\infty T_\infty}$

It is not possible to satisfy all these scaling parameters simultaneously using cold air. Momentum flux ratio along with exit pressure ratio can be matched simultaneously, but the velocity ratio cannot, requiring either a simulant gas other than air and/or high temperatures. When using cold air, one is trading lower mass flow at high velocities in flight for higher mass flow moving at slower velocities in the wind tunnel. The significance of the entrainment process is configuration dependent; in many situations the blockage effect is predominant. In the remainder of this paper the nozzle design process and scaling methodologies used will be discussed, and representative examples of predicted flight (CFD), predicted wind tunnel (CFD), and measured wind tunnel forces and moments and plume flowfields will be used to assess the effectiveness of the scaling approaches.

## II. Computational Tools

Several computational codes of varying complexity were used in the nozzle design effort. The PLUME<sup>6-7</sup> code is a simple program for computing plume boundaries of jets exhausting in to a quiescent medium for given nozzle exit conditions. It is used in this paper to illustrate effects of varying specific heat ratio, exit Mach number, and exit angle on plume shape.

The Chemical Equilibrium with Applications<sup>8-9</sup> (CEA) code was used to define nozzle exit conditions. All of the scaling methodologies are based on matching ratios of jet exit-to-freestream conditions between wind tunnel and flight conditions. The CEA program computes the chemical equilibrium compositions of complex mixtures for assigned thermodynamic states. These states are specified by two thermodynamic state functions, such as temperature and pressure or enthalpy and pressure. The CEA program then uses a minimization-of-free-energy formulation to determine the equilibrium mixture. The CEA program can also be used to solve several types of problems, including in our case the theoretical rocket performance for an infinite-area combustion chamber. Several assumptions are made in this calculation, including the one-dimensional form of the continuity, energy, and momentum equations, ideal-gas law, complete and adiabatic combustion, and isentropic expansion in the nozzle.

Computational solutions for flow over the LAV including abort motor plumes were obtained with the OVERFLOW<sup>10</sup> solver (OVERset grid FLOW). It is a compressible 3-D flow solver that solves the time-dependent, Reynolds-averaged, Navier-Stokes equations using multiple overset structured grids. Best practices for these types of flows have been developed over the course of the Orion project<sup>11-12</sup>.

### III. ACM Nozzle Design

Scaling of the ACM nozzles starts with a thrust allocation (a set of thrust values, one for each of 8 nozzles, that define resultant thrust magnitude and direction), the exit conditions of the nozzles, and the freestream conditions for flight and wind tunnel flows. First the flight nozzle exit conditions are computed with the CEA code. Next a scaling law is selected to define the nozzle exit Mach number for the wind tunnel model and isentropic relations are used to define the wind tunnel nozzle exit conditions. Then plenum conditions for the wind tunnel ACM nozzles are determined in order to match selected jet exit-to-freestream ratios. For the ACM nozzles it was decided to use overall thrust ratio (to be defined shortly) as the primary scaling parameter and matching exit conditions when possible.

The following sections describe the process in greater detail. Included are a description of the thrust allocations, determination of nozzle exit conditions, comparisons of plume shapes, and a discussion of the compromises that had to be made. Finally, comparisons of predicted flight results with wind tunnel data are made to assess the effectiveness of the scaling methodology.

#### A. Thrust Allocations

The ACM system operates as a collection of 8 nozzles in order to provide a resultant thrust from zero to a maximum value in any direction. A thrust allocation algorithm is used to define the individual nozzle thrusts necessary to obtain a specified overall thrust level and direction. Orbital Sciences, the lead subcontractor for the LAS, provided the thrust allocations in tables that contained values of resultant vacuum thrust magnitude, resultant thrust azimuth, and individual vacuum thrust values for each nozzle location. The nozzle locations are designated N1 through N8 with N1 at an azimuth angle of  $22.5^\circ$  from the top and the others following at  $45^\circ$  increments. Figure 3 shows the nozzle orientation, looking along the vehicle axis from the crew module to the nose tip.

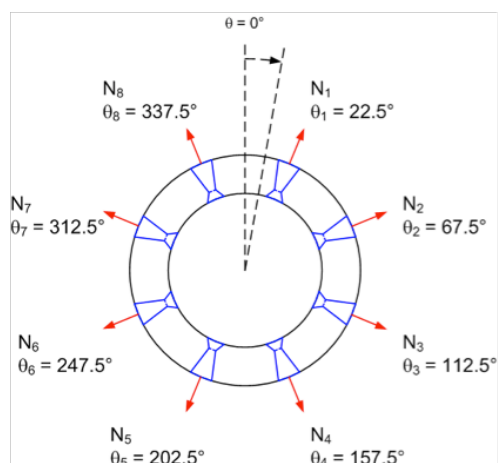


**Figure 3. Diagram of ACM nozzle locations  
(View looking along vehicle axis from crew module to nose tip)**

Figures 4 and 5 give graphical representations of the thrust allocations needed to produce three thrust levels (null thrust, mid-level thrust, maximum thrust) at azimuth angles of  $0^\circ$  and  $22.5^\circ$ . The individual thrust values have been normalized by the maximum thrust value. Note that for a zero resultant thrust, termed a null thrust condition, some of the nozzles are open and producing thrust. Null thrust is obtained by having equal thrust produced by opposing nozzles. This is required to maintain an acceptable pressure level in the combustion chamber since the propellant is always burning. These six allocations are but a small subset of what is essentially an infinite number of allocations, as the system is designed to provide thrust at any level between null and max at any azimuth angle.

To uniquely define a thrust allocation, three terms were developed to capture the thrust level and direction. Thrust ratio (also called thrust coefficient) is the non-dimensionalized total thrust along the resultant thrust direction ( $\theta_r$ ), in either direction. Thrust balance is the ratio of thrust in the direction of the resultant thrust to the total thrust

along the resultant vector, and thrust direction is the azimuth angle of the resultant thrust vector. These terms are defined as:

$$ACMTR = \frac{1}{q_\infty S} \sum_{i=1}^8 T_{v,i} \cdot |\cos(\theta_i - \theta_r)| \quad (1)$$

$$ACMTB = \frac{\sum_{j=1}^8 T_{v,j} \cdot |\cos(\theta_j - \theta_r)|}{\sum_{j=1}^8 T_{v,j} \cdot |\cos(\theta_j - \theta_r)|} \quad 270^\circ \leq |\theta_j - \theta_r| \leq 90^\circ \quad (2)$$

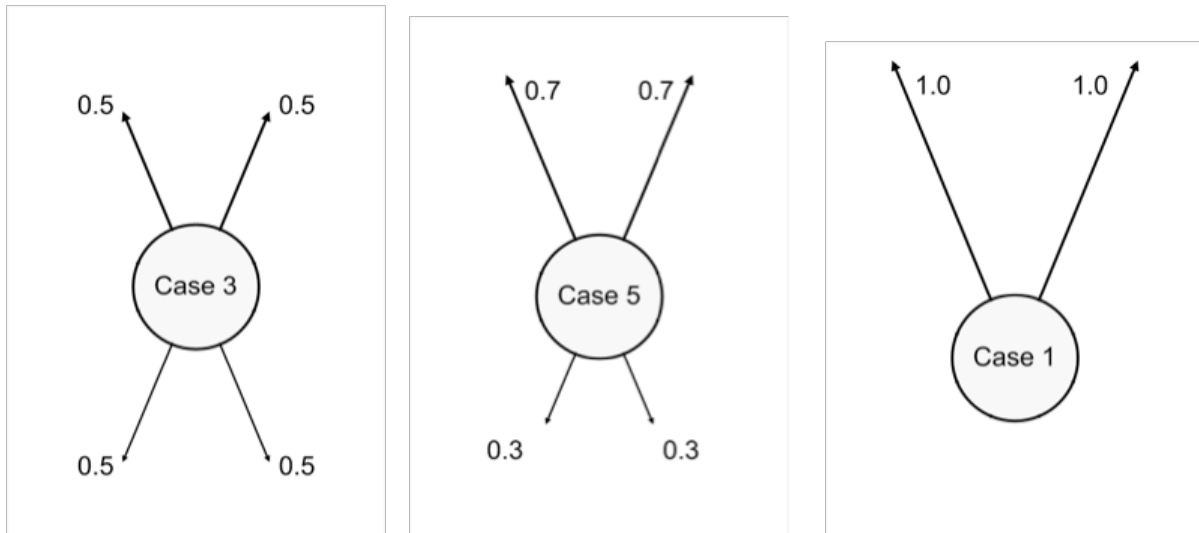


Figure 4. 0° azimuth thrust allocations; null, mid-level, maximum thrust (left to right)

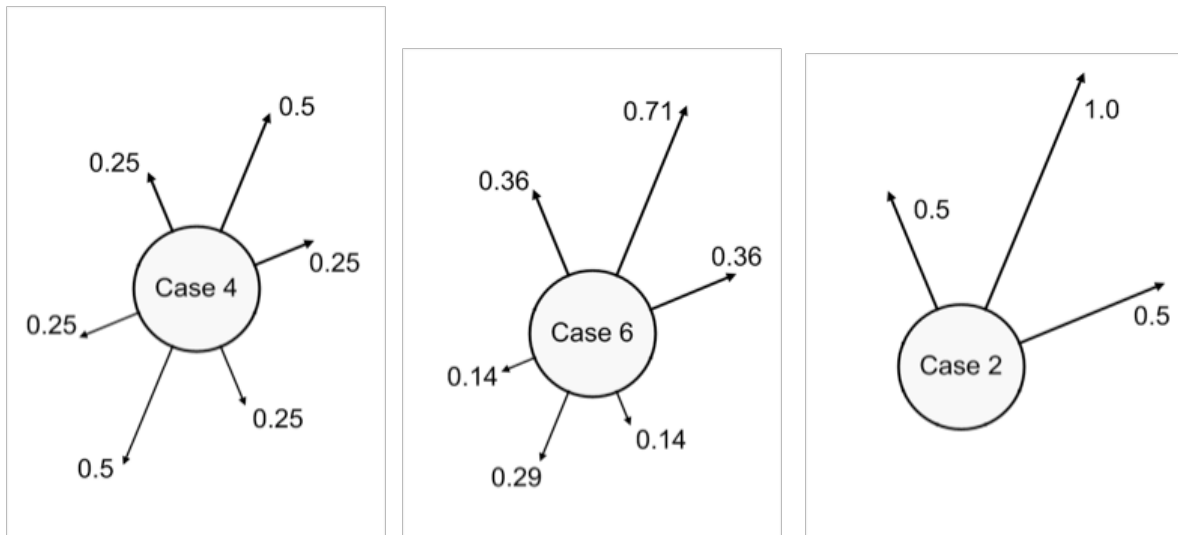


Figure 5. 22.5° azimuth thrust allocations; null, mid-level, maximum thrust (left to right)

## B. Exit Plane Conditions

The CEA code described earlier was used to define the nozzle exit conditions. The inputs to the code are the chamber pressure, the expansion ratio, and the chemical constituents of the propellant. The chamber pressure and expansion ratio were provided by Orbital as a simplified equation relating thrust to chamber pressure and throat area (valve area). Given the chamber pressure, values of throat area and thus nozzle expansion ratio are determined for each thrust level. The output of the CEA code includes the exit plane pressure, temperature, specific heat ratio, molecular weight, and Mach number. From these, momentum flux, mass flow, and thrust can be calculated. It was determined that running the CEA code at 80-93% of the nominal chamber pressure gave better agreement to the nominal thrust levels. Using these reduced chamber pressures the differences between the CEA-computed thrust and the nominal values was less than  $\pm 1.3\%$ .

## C. Plume Shapes

Plume shapes predicted by the PLUME code for flight and for several scaling methods are shown in Figs. 6a-c. Each plot is at a different exit pressure ratio condition, representative of flight at freestream Mach numbers of 0.5, 1.3 and 2.5. These conditions span the Mach number range for wind tunnel tests 59-AA and 75-AA. The thrust coefficient, defined as  $T_v/(q_\infty S)$ , is the same for all cases. It is seen that simply geometrically scaling the nozzle while changing the specific heat ratio gives plumes that are significantly smaller in diameter than the flight prediction. The two non-geometrically-scaled approaches give similar results to each other, although neither provides an exact match to the flight case, lying about halfway between the geometric scaled nozzles and flight. The effect of increasing the exit angle from  $5^\circ$  to  $15^\circ$  is shown in Fig. 6b. While not making a large difference in maximum plume diameter the initial plume region agrees much better. Lastly, note the dramatic increase in plume size as the freestream Mach number and exit pressure ratio increases (due to static pressure decreasing).

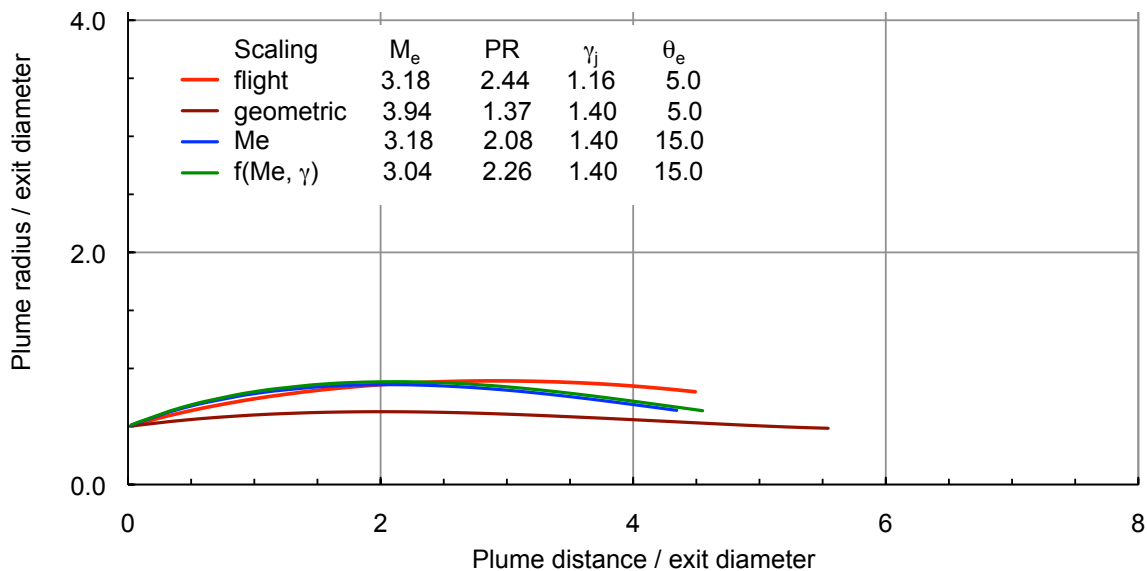


Figure 6a. Plume boundaries for  $M_\infty = 0.5$  simulation,  $C_{T,v} = 0.11$

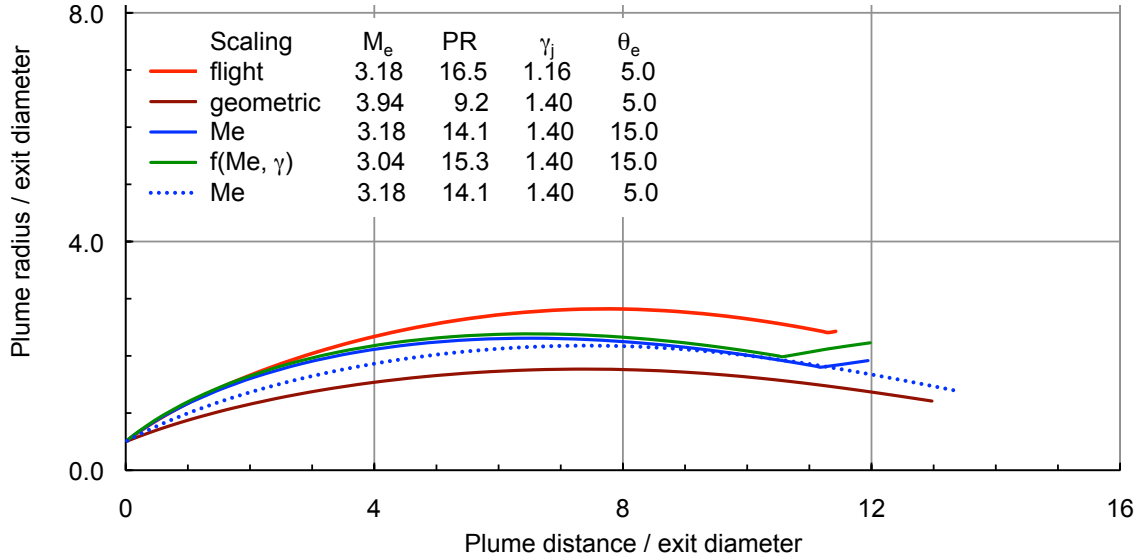


Figure 6b. Plume boundaries for  $M_\infty = 1.3$  simulation,  $C_{T,v} = 0.11$

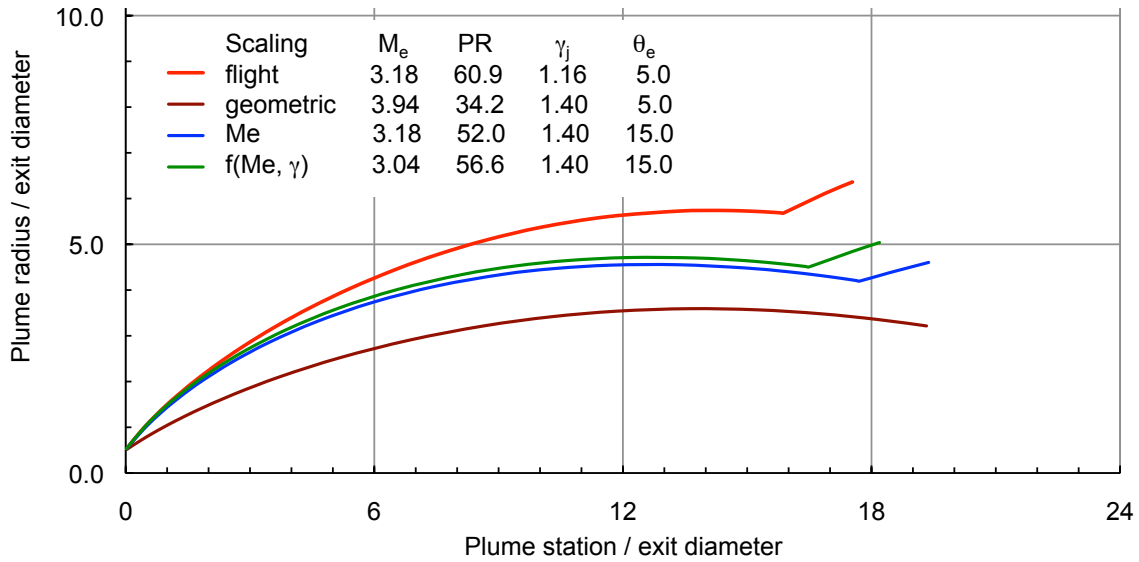
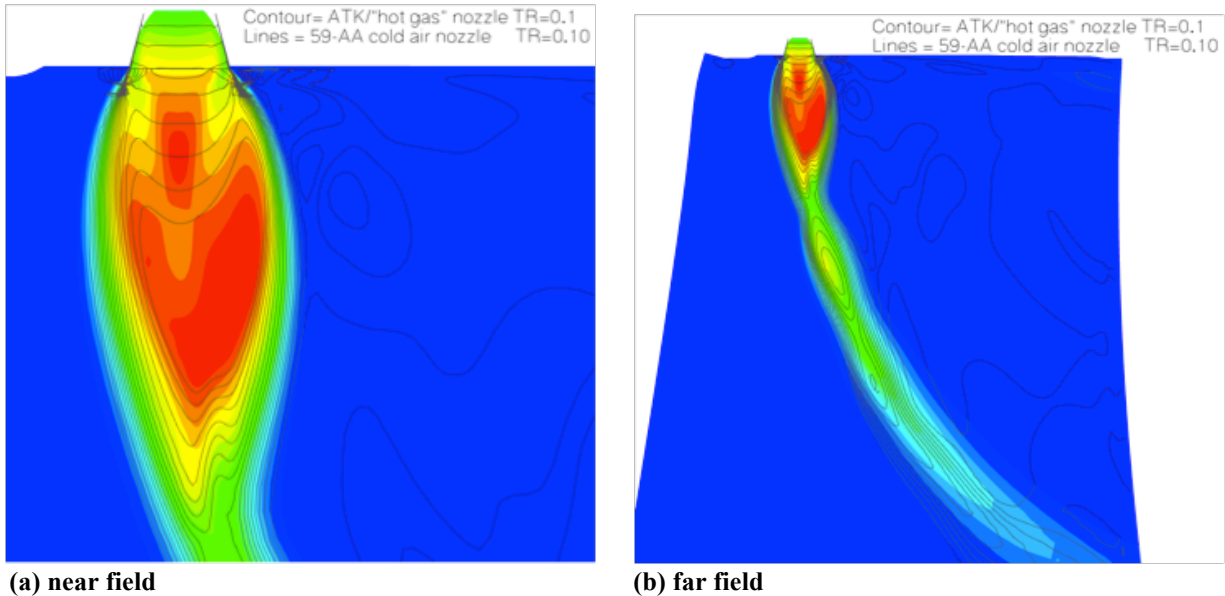


Figure 6c. Plume boundaries for  $M_\infty = 2.5$  simulation,  $C_{T,v} = 0.11$

A comparison between plume shapes predicted by the OVERFLOW CFD solver for the case of a moving freestream is shown in Fig. 7. The comparison is for a freestream Mach number of 0.5, angle of attack of  $0^\circ$ , and a thrust ratio of 0.10. The color contours are Mach number for the flight case, and the black contour lines are the cold gas wind tunnel predictions. In both the near field around the exit and the far field where the turning of the plume by the freestream flow is evident the agreement appears very good.



**Figure 7. Comparison of flight and wind tunnel plume Mach contours (both CFD),  $M_\infty = 0.5$ ,  $C_T = 0.10$**   
**Colored contours are flight “hot gas”, lines are wind tunnel cold gas**

#### D. Nozzle Design and Compromises

For the ACM nozzles the primary scaling parameter was the resultant vacuum thrust ratio, as well as thrust balance and thrust direction, all defined previously. Additionally it was desired to maintain the relative strengths of the various jets. The nominal nozzle geometry was chosen to be a conical diverging nozzle with an exit diameter geometrically scaled from the flight value, and an exit half-angle of  $15^\circ$ . For the initial CAP ACM wind tunnel test (test 59-AA) it was decided to match exit Mach number ( $M_e$ ). This was later modified for a follow-on test (test 75-AA) to use an average of  $M_e$  and  $\gamma M_e^2$ ; a compromise between conflicting opinions.

The major difficulty with this approach was the constraint of a single plenum chamber feeding all nozzles with a common pressure, arising mainly for allocations with several thrust levels. This constraint forced several nozzles to be modified (usually by lowering exit Mach number and/or reducing exit and throat areas) in order to match the overall thrust ratio. A compromise design was achieved that minimized differences in individual exit pressure ratios and thrust ratios, and maintained relative jet strength (ratio of one jet thrust to another). Another issue was liquefaction of the air in the nozzle. To alleviate this concern the static temperature at the nozzle exit was kept above the air liquefaction temperature by limiting the nozzle exit Mach number and thus the flow expansion. No attempt was made to limit liquefaction in the external plume.

As an example consider the case of maximum thrust at an azimuth angle of  $22.5^\circ$  (case 2 in Fig. 5), for a freestream Mach number of 0.5. The initial step is to determine the nozzle geometry (throat area) of the two wind tunnel nozzles by matching the exit Mach number function (either  $M_e$  or  $[M_e + \gamma M_e^2] / 2$ ) between flight and the wind tunnel (there are actually three nozzles but two are the same). Then the plenum pressures necessary to match the individual thrust ratios are determined. If it were possible to have separate plenums for the different nozzles this would automatically satisfy the overall thrust ratio equation. However, the plenum pressures in this case are different by about 30%. When a common pressure is used for the three nozzles then the match with resultant thrust ratio is no longer met. It is possible to match the thrust ratio by reducing the common plenum pressure, but then the relative strength of the jets will not be maintained, and depending on the configuration the azimuth angle will not be matched. In order to maintain the relative strength of the jets with a common plenum pressure it is necessary to reduce the thrust of the secondary nozzles. This is achieved by reducing the throat area, but then the exit Mach number is increased. A limit of 3.40 was imposed on the increase in exit Mach number due to liquefaction concerns, as the supply air is unheated. This was deemed sufficient to avoid liquefaction in the nozzles but not necessarily in the expanding plumes outside of the nozzles. If necessary both the exit and throat diameters were reduced in order to maintain relative jet strength. The smaller plume that results from the reduced exit area is somewhat compensated

for by the fact that the exit pressure ratio is increased and a higher exit pressure ratio gives a larger plume diameter. Table 1 summarizes the process for the case just described. Listed are the individual nozzle exit Mach numbers, the differences in the individual vacuum thrust and exit pressure ratios compared to the flight values (TRerr and PRerr), the jet relative strengths (RS, jet thrust divided by maximum jet thrust), and the exit diameter ratio (DR, exit diameter divided by maximum exit diameter).

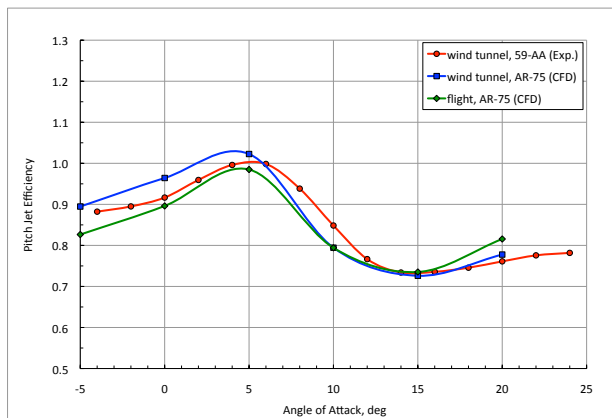
Table 1. Summary of nozzle design for case 2

Nozzle	Me	TRerr	PRerr	RSflight	RSwt	DR
1a	3.040	-13.7	-19.7	1.00	1.00	1.00
2a	3.463	19.6	9.1	0.50	0.70	1.00
1b	3.040	0.33	-6.7	1.00	1.00	1.00
2b	3.463	-0.39	38.8	0.50	0.49	0.82

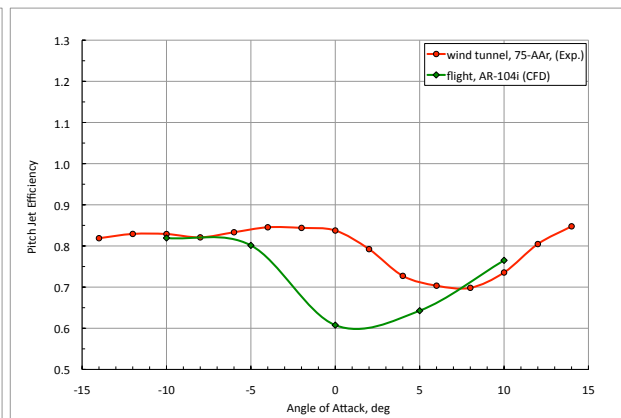
1a, 2a: common plenum pressure, no modification to secondary nozzle  
 1b, 2b: common plenum pressure, modified secondary nozzle

### E. ACM Nozzle Design Post-Test Comparisons

Figures 8a-d show representative examples of the success of the scaling process. Measured wind tunnel data from tests 59-AA and 75-AA<sup>13</sup> and predicted values from CFD are compared. Plots of jet pitching moment efficiency are shown for a maximum-thrust south-firing jet at freestream Mach numbers of 0.7, 0.9, 1.3, and 2.5. Jet efficiency is defined as the ratio of actual jet effectiveness to nominal (no interaction) jet effectiveness. Values less than one indicate an attenuating jet, providing less control authority than for a jet with no interaction, while values greater than one indicate an augmenting jet interaction. Angles of attack range from  $-14^\circ$  to  $14^\circ$  resulting in a jet firing into the leeside flowfield as well as the windward flowfield. At Mach 0.7 the predicted variation between wind tunnel and flight is shown (curves labeled AR-75), as well as the measured wind tunnel data (labeled 59-AA). These data are for the -068 configuration while the subsequent plots are for the ALAS configuration. The predicted differences between flight and wind tunnel simulation is only significant for low angles of attack. The agreement between measured wind tunnel results and flight prediction is very good, within 6% at all angles of attack. At the higher Mach numbers the CFD was not run for wind tunnel conditions, only flight. At Mach 0.9 the agreement is again good, except for  $\alpha = 0^\circ$  where differences in jet efficiency approach 23%. Whether this is a true error or due to mis-characterization in the wind tunnel plumes or the computed plumes is not resolved. At the higher Mach numbers the wind tunnel predicts more attenuation or less augmentation than the CFD flight predictions, but the differences are no more than 9%.



(a)  $M_\infty = 0.7$ , ACMTR = 0.10, -068 configuration



(b)  $M_\infty = 0.9$ , ACMTR = 0.05, -ALAS configuration

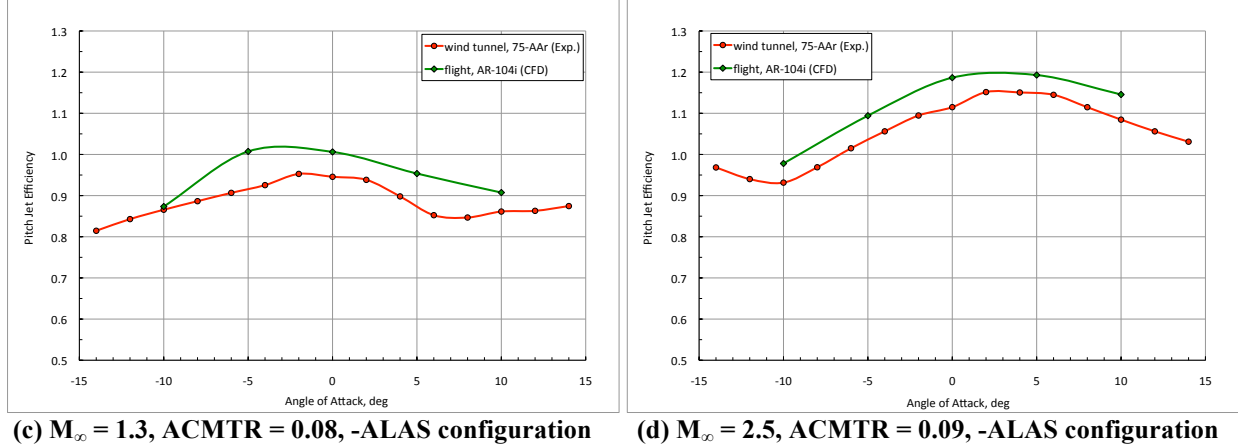


**Figure 8. Comparison of predicted and measured pitch jet efficiency,  $ACMTB = 1.0$ ,  $ACMTHETA = 180$  (south-firing jet)**

#### IV. AM Nozzle Design

Scaling the nozzles for the abort motor test was anticipated to be more troublesome than the ACM nozzles due to the proximity of the plumes to the vehicle surface, with plumes aligned roughly along the vehicle longitudinal axis as opposed to perpendicular as with the ACM plumes, and due to possible mixing or entrainment effects. As this interaction was thought to involve more than plume blockage, and with the pre-imposed limitation of cold air as the test gas, it was decided to incorporate CFD in selecting the best scaling methodology, and to base that selection on minimizing the error between wind tunnel and flight predictions of total aerodynamic coefficients.

##### A. CFD Scaling Study Inputs

For the CFD study, various scaling parameters were used to define the nozzle geometries (primarily expansion ratio (function of exit Mach number) and exit angle), and then CFD calculations were made for a limited set of Mach numbers and angles of attack. The scaling parameters used are listed below in table 2. The  $\gamma_j M_e^2$  scaling parameter was used in the ACM design analysis and will match momentum and exit pressure ratios simultaneously. The  $\gamma_j M_e^2 / \beta_j$  scaling parameter is similar, but the derivation incorporates the initial plume angle as well. The fully-expanded-plume  $q_{fe}$ -ratio scaling was thought to be relevant as the plumes would be nearly fully expanded in the vicinity of the LAS ogive and thus might give a reasonable approximation of the impingement and near-impingement effects. In addition to the exit Mach number function, thrust coefficient along the vehicle centerline was matched, as well as a thrust offset of  $0.5^\circ$ .

Table 2. Scaling parameters used for 26-AA nozzle design

Exit Mach number function:  $\gamma_j M_e^2$

$\gamma_j M_e^2 / \beta_j$

$M_{fe}$  *Mach number required to expand nozzle flow to freestream static pressure*

AMCT:  $\frac{1}{q_\infty S} \sum_{i=1}^4 T_{v,i} \cos(25^\circ)$  *where  $\sum_{i=1}^4 T_{v,i}$  is total vacuum thrust along longitudinal axis*

$q_{fe}$ -ratio:  $q_{fe} / q_\infty$  *where  $q_{fe} = (\gamma_j P_\infty M_{fe}^2) / 2$  and represents conditions in a plume fully expanded to freestream pressure*

The computational solutions were obtained with the OVERFLOW solver. All computational cases, at either flight or wind tunnel conditions, were run at full-scale vehicle dimensions with the same freestream static and dynamic pressures so that the only difference was plume modeling. The flight plume was modeled as a calorically-perfect gas with a specific-heat ratio of approximately 1.2 and appropriate values of molecular weight and total temperature. The wind tunnel plume was modeled as a calorically-perfect gas with a specific-heat ratio of 1.40, molecular weight for air, and a total temperature of 560 °R. These analyses were performed using the 26-AA wind tunnel model geometry, which represented the LAS-606-E configuration but where the abort motor nozzle OML was modified to allow a larger internal plenum area and to accommodate the larger throat diameters required by the scaling methods. Figure 9 shows the modification made to the OML.

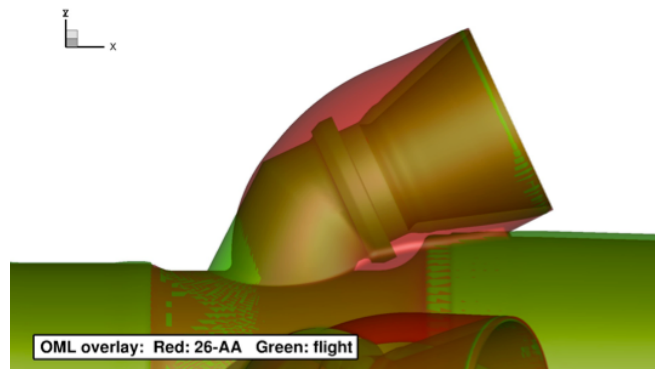


**Figure 9. Abort motor OML modifications**

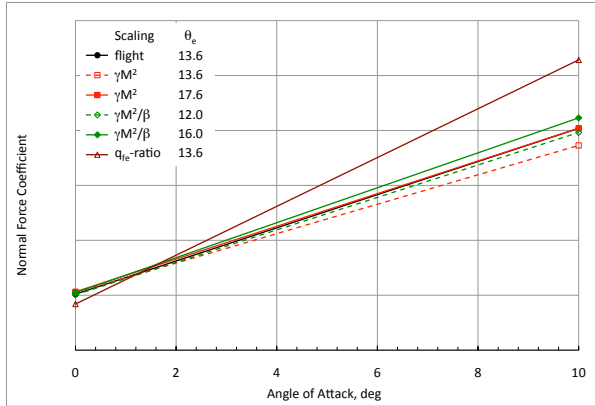
Given an exit Mach number scaling parameter, the design of the abort motor nozzles was more straightforward than that for the ACM nozzles in that limitations due to a common plenum and exit Mach number were not a factor. The nominal exit Mach numbers are low enough so that liquefaction concerns within the nozzle are not an issue. The thrust levels of the 4 nozzles are similar, so a common plenum is workable. The nozzle throat diameters still had to be modified slightly to maintain the thrust offset, but by less than 1%. As discussed further later on, the initial plume angle was seen to have a significant effect on the aerodynamic results. This angle is calculated as the sum of the nozzle exit angle and the Prandtl-Meyer expansion angle required to turn the flow from the nozzle exit pressure to the freestream pressure. The sensitivity of the simulations to this parameter was therefore assessed by including several exit angle variations. Table 3 lists the CFD cases. The wind tunnel model used conical nozzles instead of contoured nozzles, so a few cases were run at flight conditions but with conical nozzles to assess the effect of that simplification, which was small.

Table 3. Case matrix for CFD-based scaling selection

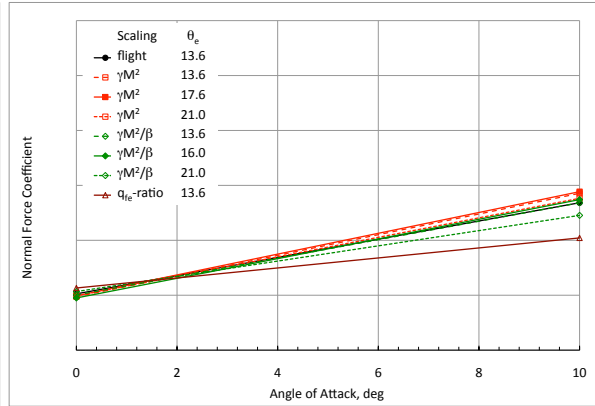
$M_\infty$	AMCT	Scaling ( $M_e$ function)	$q_\infty$ (psf)	$\alpha$ (deg)	$\theta_e$ (deg)
1.3	4.0	flight	462	0, 10	13.6
1.3	4.0	flight, conical	462	0, 10	13.6
1.3	4.0	$\gamma_j M_e^2$	462	0, 10	13.6, 17.6
1.3	4.0	$\gamma_j M_e^2 / \beta_j$	462	0, 10	12.0, 16.0
1.3	4.0	$q_{fe}$ -ratio	462	0, 10	13.6
3.0	6.0	flight	308	0, 10	13.6
3.0	6.0	flight, conical	308	0, 10	13.6
3.0	6.0	$\gamma_j M_e^2$	308	0, 10	13.6, 17.6, 21.0
3.0	6.0	$\gamma_j M_e^2 / \beta_j$	308	0, 10	13.6, 16.0, 21.0
3.0	6.0	$q_{fe}$ -ratio	308	0, 10	13.6
0.7	6.0	flight	308	0, 10	13.6
0.7	6.0	$\gamma_j M_e^2$	308	0, 10	13.6, 17.6
0.7	6.0	$\gamma_j M_e^2 / \beta_j$	308	0, 10	12.0, 16.0
4.6	14.0	flight	132	0, 10	13.6
4.6	14.0	$\gamma_j M_e^2 / \beta_j$	132	0, 10	16.0, 21.0

## B. CFD Scaling Study Results

Results of the plume scaling study in terms of force-and moment coefficients are shown in Figs. 10-12. Normal-force, axial-force, and pitching-moment coefficients are shown for Mach numbers of 1.3 and 3.0, the initial values used in the study. The fully-expanded  $q_{fe}$ -ratio scaling resulted in poor agreement with the flight predictions at both Mach numbers, and this method was dropped from further consideration. The wind tunnel-to-flight agreement using the  $\gamma_j M_e^2$  scaling with exit angle of  $13.6^\circ$  was good at Mach 1.3 but poor at Mach 3.0. Some of the reasons for these results can be seen in Figs. 13 and 14, which show Mach number contours of the flowfield along with streamline traces within the plumes. The plumes for the  $q_{fe}$ -ratio scaling lie too close to the body at Mach 1.3 (Fig. 13a), while at Mach 3.0 (Fig. 13b) the nature of the wake region is altered. The  $\gamma_j M_e^2$  scaling approximates the plume shapes correctly, but as seen at Mach 3.0 the separation in front of the AM is not captured correctly. This discrepancy at Mach 3.0 led to the addition of the  $\gamma_j M_e^2 / \beta_j$  scaling cases and the nozzle exit angle variations, as it was thought that getting the initial plume angle correct would lead to better modeling. It does appear that the upper tower separation is modeled more accurately with the  $\gamma_j M_e^2 / \beta_j$  scaling ( $\theta_e = 16.0^\circ$ ) at both Mach 1.3 and 3.0 and the pitching moment comparisons with flight prediction are better. The use of  $\gamma_j M_e^2$  scaling with an exit angle of  $17.6^\circ$  provided a slightly better comparison at Mach 1.3 than  $\gamma_j M_e^2 / \beta_j$  scaling with an exit angle of  $16.0^\circ$ , but was worse at Mach 3.0.

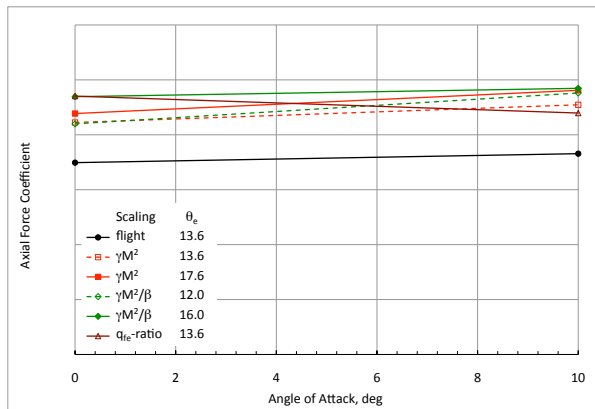


(a)  $M_{\infty} = 1.3$ , AMCT = 4

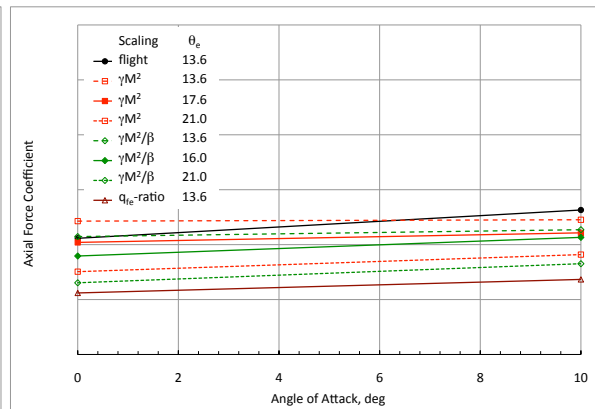


(b)  $M_{\infty} = 3.0$ , AMCT = 6

Figure 10. Force-and-moment characteristics for several scaling methodologies (normal force)

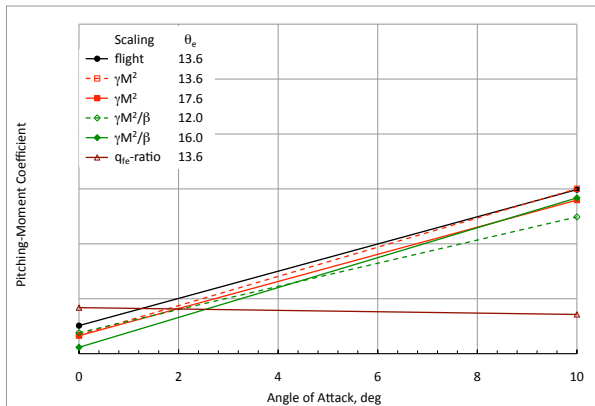


(a)  $M_{\infty} = 1.3$ , AMCT = 4

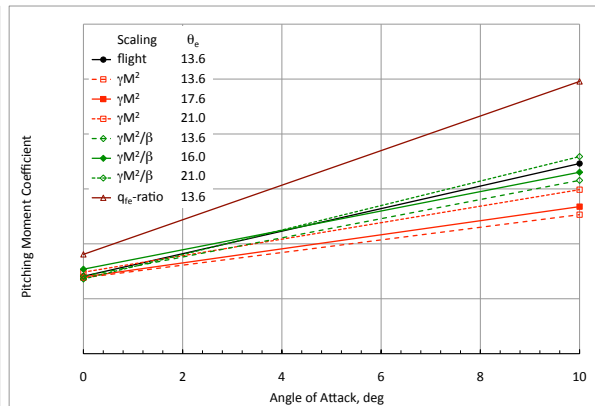


(b)  $M_{\infty} = 3.0$ , AMCT = 6

Figure 11. Force-and-moment characteristics for several scaling methodologies (axial force)



(a)  $M_{\infty} = 1.3$ , AMCT = 4



(b)  $M_{\infty} = 3.0$ , AMCT = 6

Figure 12. Force-and-moment characteristics for several scaling methodologies (pitching moment)

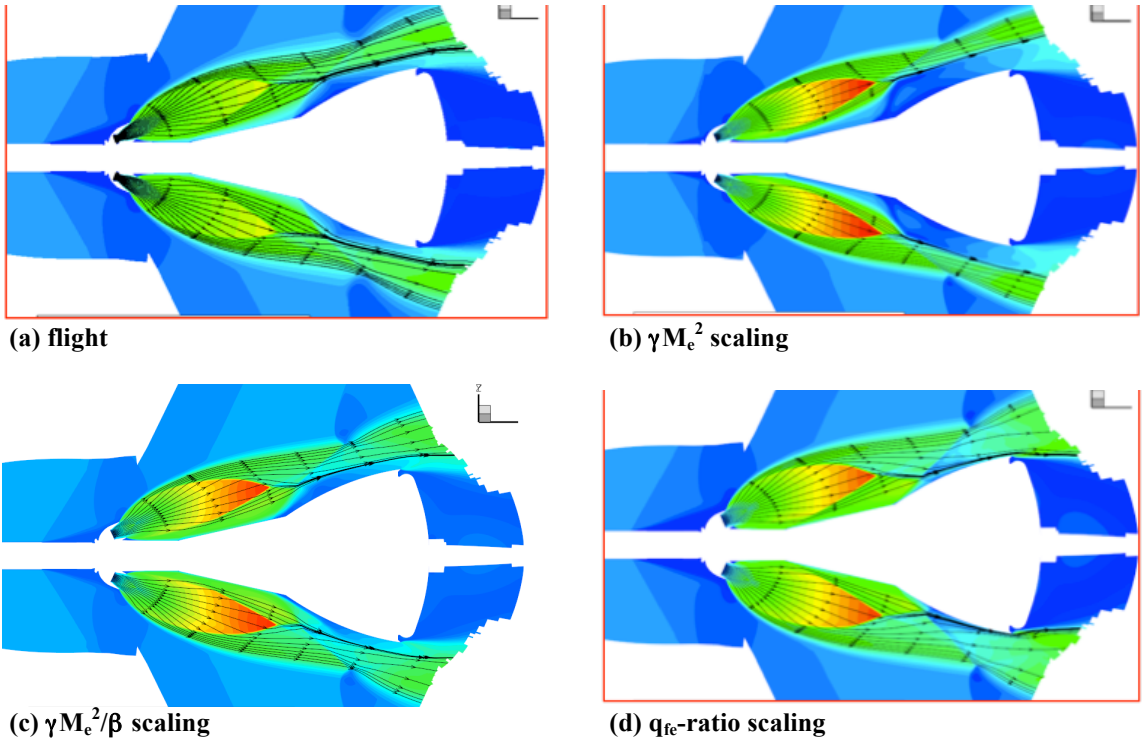


Figure 13. Mach number contours and plume streamline traces for several scaling methodologies,  $M_\infty = 1.3$

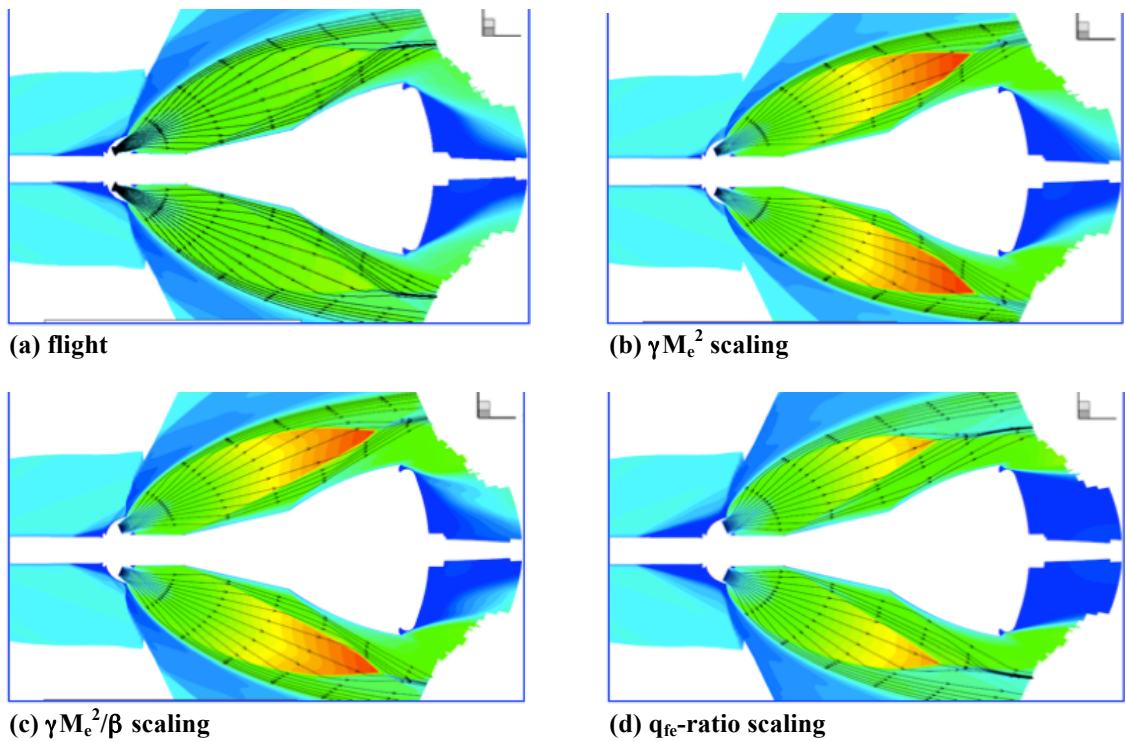
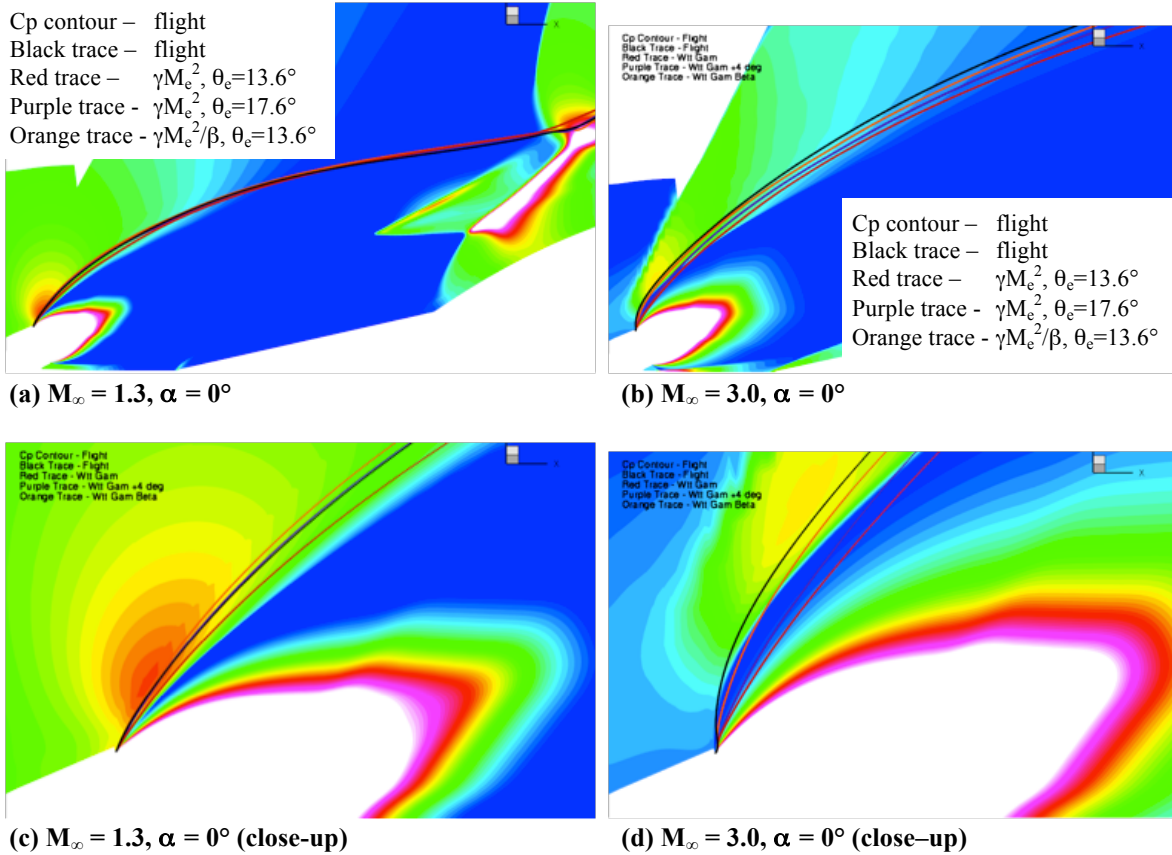


Figure 14. Mach number contours and plume streamline traces for several scaling methodologies,  $M_\infty = 3.0$

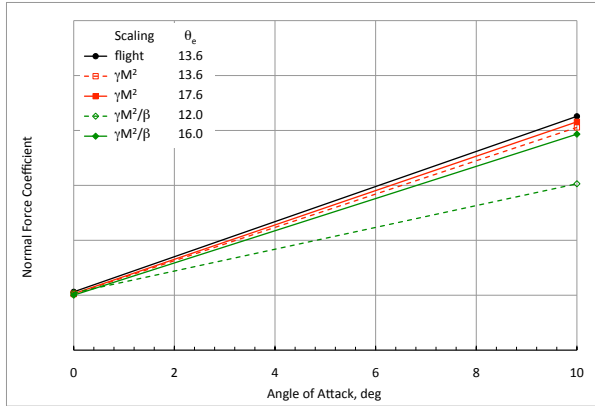
A more detailed look at the plume boundaries is shown in Fig. 15a-d. The figures show flight flowfield pressure contours with traces of the plume boundary for the various scaling methods. At Mach 1.3, both  $\gamma_j M_e^2$  ( $\theta_e = 17.6^\circ$ ) and  $\gamma_j M_e^2/\beta_j$  scaling ( $\theta_e = 16.0^\circ$ ) approximate the plume boundary closely, with the original  $\gamma_j M_e^2$  ( $\theta_e = 13.6^\circ$ ) being somewhat inferior. At Mach 3.0,  $\gamma_j M_e^2/\beta_j$  scaling is superior in matching the flight plume.



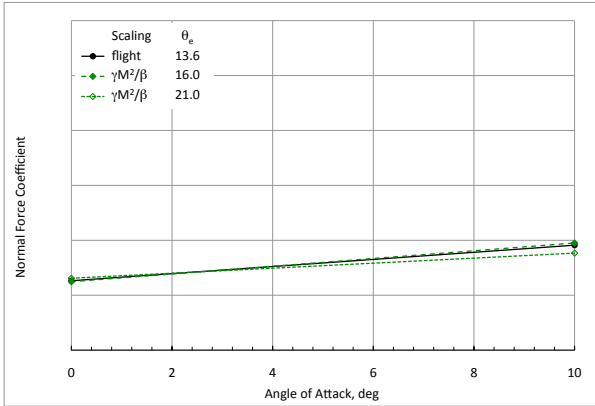
**Figure 15. Plume boundary traces for various scaling methodologies**

Additional CFD cases were run to broaden the Mach range to 0.7 and 4.6 and to further assess the effects of nozzle exit angle. As can be seen from the force-and-moment data shown in Figs. 16-18, the  $\gamma_j M_e^2/\beta_j$  scaling did not work well at the lowest Mach number, while  $\gamma_j M_e^2$  scaling did not work well at the higher two Mach numbers. Either scaling method provided satisfactory results at Mach 1.3. A final decision was then made to use different scaling methods for each test section,  $\gamma_j M_e^2$  scaling with an exit angle of  $17.6^\circ$  in the 11-ft tunnel (Mach range 0.3 to 1.3) and  $\gamma_j M_e^2/\beta_j$  scaling with an exit angle of  $16^\circ$  in the 9x7-ft tunnel (Mach range 1.6 to 2.5).

While the force-and-moment and streamline trace comparisons looked promising, when one examined the surface pressures the results were less encouraging. Figures 19-21 present delta-Cp plots at Mach 1.3 and 3.0 for  $\alpha = 0^\circ$ . The plots show the difference in surface pressure ( $C_p$ ) from the flight prediction for the various scaling methods, including the effect of changing the flight nozzle from contoured to conical. As can be seen, although the global force-and-moment results may show good agreement, the surface pressures show quite a bit of discrepancy. At Mach 1.3 the regions directly under the plumes are most affected; at Mach 3.0 the entire region from the nozzles to the midpoint of the BPC is affected due to the larger plumes. A mitigating factor may be that the flowfield is still somewhat symmetric (even at an angle of attack of  $10^\circ$  and with a thrust offset), so that there is some cancelling between the windward and leeward surfaces; there is also some balancing effect of pressures forward and aft of the moment reference center, located at approximately the cone/ogive junction. In any case, these CFD results were used to select the scaling methodology for the abort motor test (26-AA).

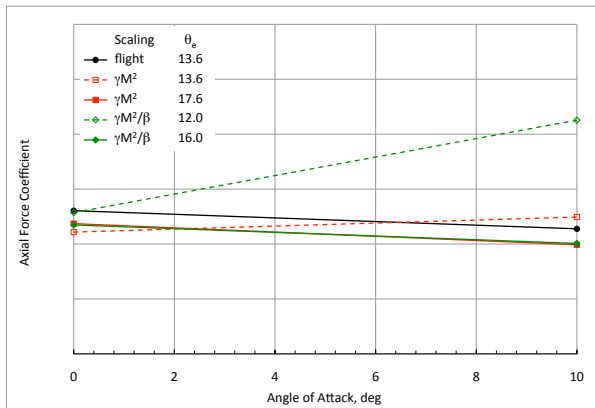


(a)  $M_\infty = 0.7$ , AMCT = 6

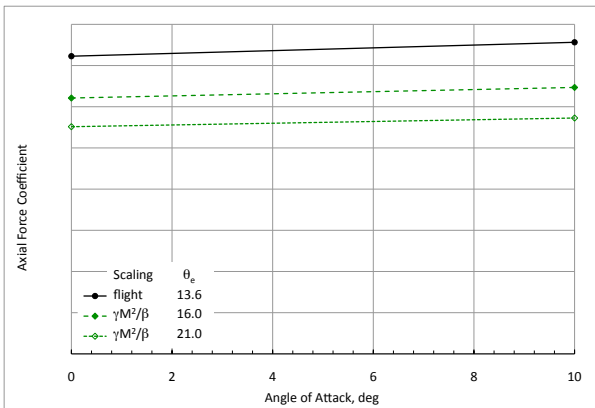


(b)  $M_\infty = 4.6$ , AMCT = 14

Figure 16. Force-and-moment characteristics for several scaling methodologies (normal force)

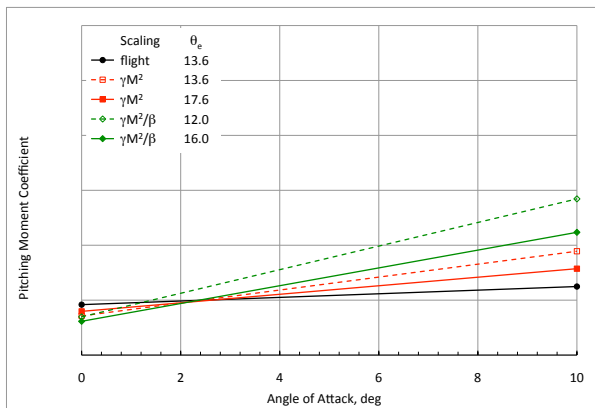


(a)  $M_\infty = 0.7$ , AMCT = 6

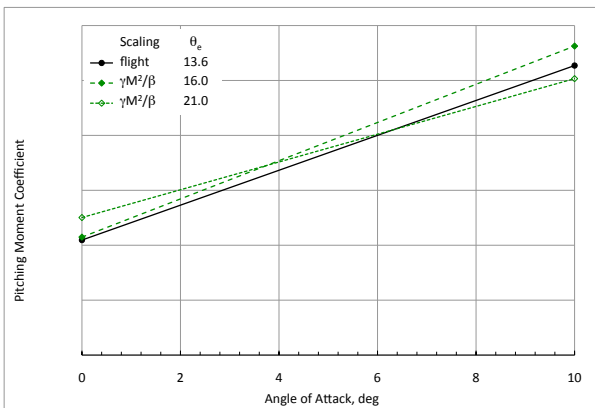


(b)  $M_\infty = 4.6$ , AMCT = 14

Figure 17. Force-and-moment characteristics for several scaling methodologies (axial force)

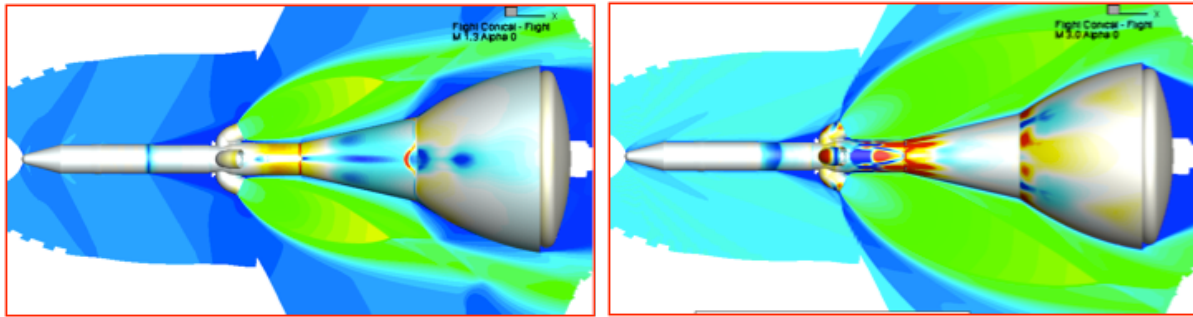


(a)  $M_\infty = 0.7$ , AMCT = 6



(b)  $M_\infty = 4.6$ , AMCT = 14

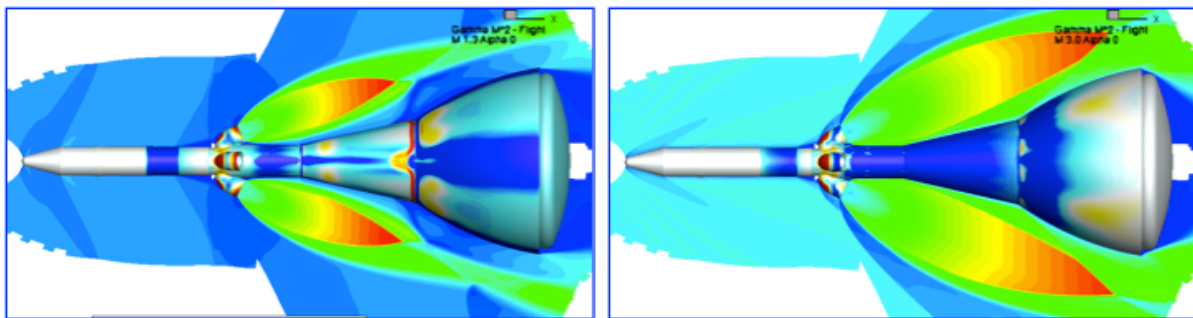
Figure 18. Force-and-moment characteristics for several scaling methodologies (pitching moment)



(a)  $M_\infty = 1.3$ , flight – flight, conical

(b)  $M_\infty = 3.0$ , flight – flight, conical

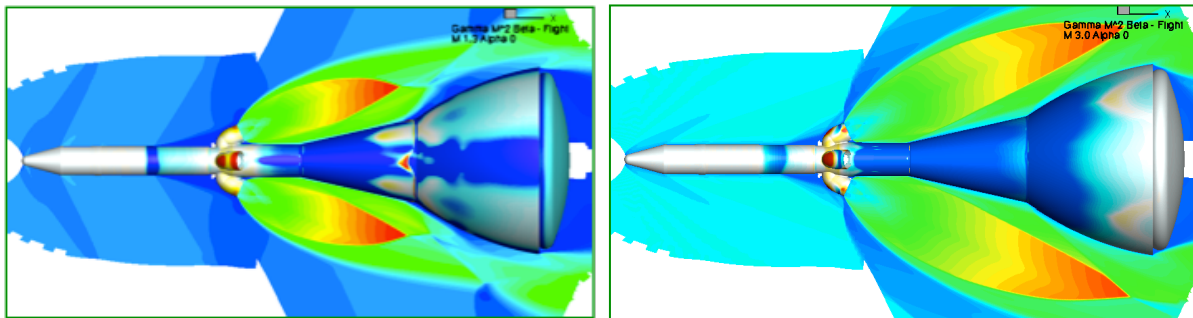
Figure 19. Differential surface pressure contours for several scaling methodologies,  $\alpha = 0^\circ$



(a)  $M_\infty = 1.3$ , flight –  $\gamma M_e^2$  scaling

(b)  $M_\infty = 3.0$ , flight –  $\gamma M_e^2$  scaling

Figure 20. Differential surface pressure contours for several scaling methodologies,  $\alpha = 0^\circ$



(a)  $M_\infty = 1.3$ , flight –  $\gamma M_e^2 / \beta$  scaling

(b)  $M_\infty = 3.0$ , flight –  $\gamma M_e^2 / \beta$  scaling

Figure 21. Differential surface pressure contours for several scaling methodologies,  $\alpha = 0^\circ$

### C. AM Nozzle Design Post-Test Comparisons

The success, or lack thereof, of this scaling approach is shown by comparison of predicted and measured pitching moment increments from test 26-AA. This test used different thrust coefficients and a different thrust offset than for the CFD scaling study so a direct comparison with those predictions cannot be made but the methodology was the same and applied to the conditions of this test. Comparisons of the predicted flight (designated AR-104), predicted wind tunnel (AR-120) and measured wind tunnel (26-AA) pitching moments are shown in Figs. 22-23 for several freestream Mach numbers. The flight geometry was different than the wind tunnel model in both the

forementioned modifications to the OML around the abort motors, and the ogive BPC (Boost Protective Cover) of the flight geometry was slightly longer. A correction for these OML differences, based on unpowered CFD, is applied to the wind tunnel data and indicated as “26-AA + AR-119”. Error bars on the adjusted wind tunnel data approximate test level uncertainties. The agreement is reasonable, generally within the test uncertainties. For all Mach numbers except Mach 2.5, the flight prediction is more stable (nose-down pitching moment for positive angles of attack). A more complete discussion of the 26-AA wind tunnel test<sup>14</sup> and the associated computational effort<sup>12, 15</sup> can be found in other papers presented at this conference.

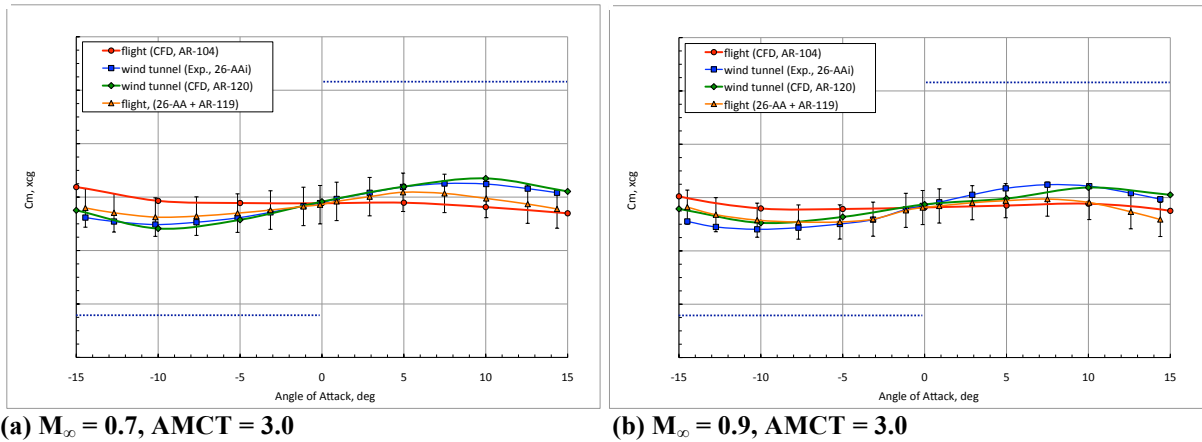


Figure 22. Comparison of predicted and measured pitching moments with abort motor interactions

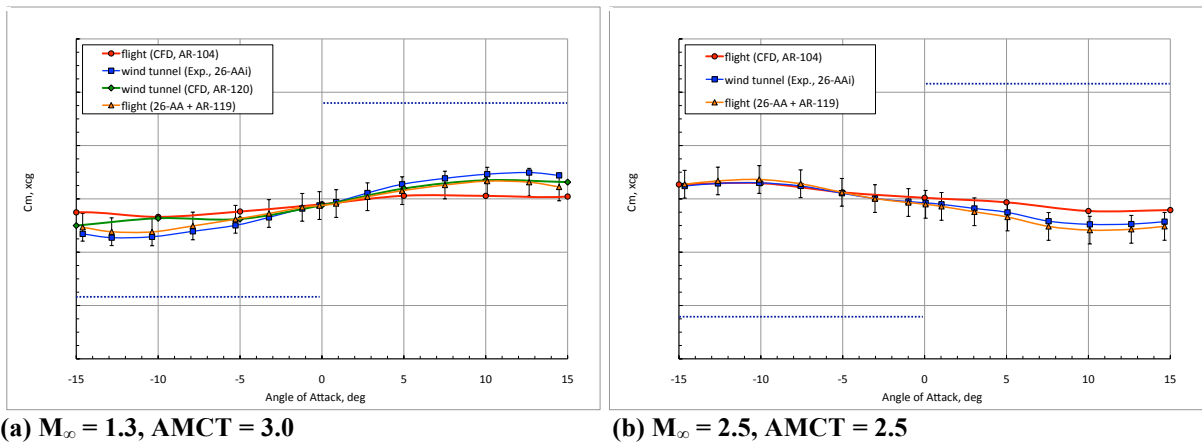


Figure 23. Comparison of predicted and measured pitching moments with abort motor interactions

## V. JM Nozzle Design

The jettison motor nozzles were designed in a similar manner to the ACM nozzles. The exit conditions for the scarfed nozzles were computed as for an axisymmetric nozzle. This is a good assumption provided the Mach angle is less than nozzle scarf angle. The CEA code was again used to determine nozzle exit conditions for the large and small JM nozzles given exit-to-throat area ratios and chamber conditions. Wind tunnel model nozzle exit Mach number was calculated to allow simultaneous matching of thrust ratio, momentum flux ratio, and static pressure ratio. Nozzle exit angle was adjusted to allow a better match of the plume boundary as predicted by the PLUME code. A more complete description of the jettison motor scaling can be found in the paper by Rhode<sup>16</sup>.

## VI. Summary

This paper described the design of nozzles for use in a wind tunnel test program to assess the interaction effects between the attitude control motor and abort motor plumes and the external flow over the LAV. The wind tunnel tests used high-pressure air as the simulant gas to model the actual rocket exhaust plumes. Proper scaling is necessary to account for the differences between flight and wind tunnel exhaust plumes and pure geometric scaling is not appropriate. The effectiveness of the various scaling methodologies was assessed by comparisons between predicted flight and predicted wind tunnel flowfields as well as comparisons between predicted flight and measured wind tunnel force-and-moment data. The scaling methodology for the ACM nozzles used either  $\gamma M_e^2$  or  $(M_e + \gamma M_e^2)/2$  to define the nozzle exit Mach number, and matched thrust ratio and relative jet strength. Reasonable agreement between measured wind tunnel data and flight predictions was obtained for the ACM interactions. The scaling methodology for the AM plumes used either  $\gamma M_e^2$  or  $\gamma M_e^2/\beta$ , depending on wind tunnel test conditions, to define the nozzle exit Mach number, and matched thrust ratio and thrust offset. Again, reasonable agreement in terms of force-and-moment coefficients were obtained between predicted flight, predicted wind tunnel, and measured wind tunnel data. However, the computational predictions did indicate somewhat large discrepancies in surface pressure between flight and wind tunnel conditions.

## References

- <sup>1</sup>Pinzola, M., "Jet Simulation in Ground Test Facilities", AGARDograph79, 1963.
- <sup>2</sup>Spaid, F. W., and Cassel, L. A., "Aerodynamic Interference Induced by Reaction Controls", AGARD-AG-173, 1973.
- <sup>3</sup>Casell, L. A., "Applying Jet Interaction Technology", *Journal of Spacecraft and Rockets*, Vol. 40, No. 4, 2003, pp. 523-537.
- <sup>4</sup>Kanipe, D. B., "Plume/Flowfield Jet Interaction Effects on the Space Shuttle Orbiter During Entry", AIAA Paper 1982-1319, August 1982.
- <sup>5</sup>Cassel, L. A., Shivananda, T., Feiz, H., Kovacic, S., and Douglas, R., "Reverse Flow Plume Interference Wind Tunnel Testing For CEV Launch Abort System (LAS)", AIAA Paper 2008-347, January 2008.
- <sup>6</sup>Salas, M. D., "The Numerical Calculation of Inviscid Plume Flow Fields", AIAA Paper 1974-0523, June 1974.
- <sup>7</sup>Scallion, W. I., "Effects of Nozzle Exit Geometry and Pressure Ratio on Plume Shape for Nozzles Exhausting into Quiescent Air", NASA TM-104097, May 1991.
- <sup>8</sup>Gordon, S., and McBride, B. J., "Computer Program for Calculation of Complex Chemical Equilibrium Compositions and Applications, I. Analysis", NASA RP-1311, October 1994.
- <sup>9</sup>McBride, B. J., and Gordon, S., "Computer Program for Calculation of Complex Chemical Equilibrium Compositions and Applications, II. Users Manual and Program Description", NASA RP-1311, June 1996.
- <sup>10</sup>Jespersen, D., Pulliam, T., and Buning, P., "Recent Enhancements to OVERFLOW", AIAA Paper 97-0644, January 1997.
- <sup>11</sup>Chaderjian, N. M., and Olsen, M.E., "CEV CFD Simulation Guidelines for the OVERFLOW 2 Navier-Stokes Solver", NASA Ames Research Center, Rept. EG-CAP-06-33, Moffett Field, CA, August 2006.
- <sup>12</sup>Childs, R., Garcia, J. A., Rogers, S. E., Shestopolov, A., and Vicker, D., "Overflow Simulation Guidelines for Orion Launch Abort Vehicle Aerodynamic Analyses", 29<sup>th</sup> Applied Aerodynamics Conference, AIAA, Hawaii (submitted for publication).
- <sup>13</sup>Murphy, K. J., Brauckmann, G. J., Walker, E. L., Chan, D. T., and Foley, R. J., "Orion Launch Abort Vehicle Attitude Control Motor Testing", 29<sup>th</sup> Applied Aerodynamics Conference, AIAA, Hawaii (submitted for publication).
- <sup>14</sup>James, K., Storms, B., Ross, J., Martwick, F., Morr, D., Ryle, S., Walker, E., and Foley, R., "Orion Launch Abort Vehicle Abort Motor Testing", 29<sup>th</sup> Applied Aerodynamics Conference, AIAA, Hawaii (submitted for publication).
- <sup>15</sup>Rogers, S. E., and Pulliam, T. H., "Computational Challenges in Simulating Powered Flight of the Orion Launch Abort Vehicle", 29<sup>th</sup> Applied Aerodynamics Conference, AIAA, Hawaii (submitted for publication).
- <sup>16</sup>Rhode, M. N., Niskey, C., Wilson, M., and Chan, D., "Aerodynamic Testing of the Orion Launch Abort Tower Separation with Jettison Motor Jet Interactions", 29<sup>th</sup> Applied Aerodynamics Conference, AIAA, Hawaii (submitted for publication).